JCAMECH

Vol. 51, No. 1, June 2020, pp 144-156
DOI: 10.22059/jcamech.2020.294821.464

An Analytical Solution for Temperature Distribution and Thermal Strain of FGM Cylinders with Varying Thickness and Temperature-Dependent Properties Using Perturbation Technique

Mohammad Parhizkar Yaghoobi and Mehdi Ghannad *

Faculty of Mechanical and Mechatronics Engineering, Shahrood University of Technology, Semnan, Iran

ARTICLE INFO

Article history:
Received: 28 December 2019
Accepted: 20 May 2020

Keywords:
Analytical Solution
Temperature Distribution
Thermal Strain
Cylinders with Varying Thickness
Temperature-Dependent Properties
Functionally Graded Material (FGM),
First-Order Temperature Theory (FTT)
Perturbation Technique

ABSTRACT

This research presents temperature distribution and thermal strain of functionally graded material cylinders with varying thickness and temperature-dependency properties that are subjected to heat fluxes in their inner and outer layers. The heterogeneous distribution of properties is modeled as a power function. Using first-order temperature theory and the energy method, governing equations are extracted. The system of governing differential equations is a system of nonlinear differential equations with variable coefficients, which are solved by using the analytical method of the matched asymptotic expansion of the perturbations technique. Results obtained from temperature distribution, heat flux, and thermal strain for different heterogeneous constants and temperature-dependency properties are discussed. They show that heterogeneity has a significant impact on the temperature field and thermal strain inside functionally graded cylinders. Moreover, it is observed that heterogeneity has no impact on the direction of heat flux vector inside the body; however, any changes in heterogeneity would change the magnitude of heat flux. The results obtained from the analytical method were compared with those of previous studies and FEM, which showed good agreement.

1. Introduction

Functionally graded materials (FGMs) have been made to improve the behavior of structure towards high temperature while increasing the thermal resistance of the structure. These materials which are heterogeneous have better properties due to gradual changes in the distribution of properties compared to conventional composite materials, and their stresses and its changes in these materials form a continuous part that increases the strength of these materials compared to other common materials. Since these materials are often made of metal-ceramic composites, and their properties change from ceramic phase to metal continuously from one surface to another they can withstand high temperatures and are one of the most widely used materials for use under thermal loading and are widely used in high temperature environments [1-5].

Zimmerman and Lutz [6] obtained the exact solution of functionally graded (FG) cylinders which were subjected uniform heat under plane strain conditions. In this research, the radial and circumferential stresses were investigated and the thermal expansion coefficient for the FG cylinder was calculated. The distribution of temperature and thermal stresses of FG cylinders that were transient cooling on their inner surface was presented by Awaji and Sivakumar [7]. The results related to the thermal stresses and transient temperature were evaluated and drawn in the cooling state of the inner layer of the cylinder. El-Naggar et al. [8] obtained a solution of transient thermal stresses in heterogeneous and anisotropic (orthotropic) rotary cylinders using numerical method. The semi-analytic solution of thermo-elasticity of FG finite length cylinders was presented by using the multi-layered method by [9-10]. Using a multi-layer method, they converted the FG cylinder into homogeneous cylinders that were in contact with each other, and then, by applying the conditions of continuity at the contact surface of the cylinders, they solved their thermo-elasticity. A one-dimensional thermo-elastic transient analysis of FG cylinders was carried out using the Laplace transform [11-12]. Bahtui and Eslami [13] obtained the coupled thermo-elasticity analysis of FG cylinders with finite length. They extracted the final coupled thermo-elasticity solution of FG cylinders under thermal shock. An asymmetric thermo-elastic analysis of long cylinders made of FGM was investigated by considering the heat transfer as one-dimensional (in the direction of cylinder thickness) and two-dimensional (in radial and circumferential directions) by [14] and [15], respectively. The results of the displacements, stresses and temperature were compared and evaluated. A one-dimensional stable and transient thermo-elastic analysis of FG cylinders was presented using Fredholm integral method by Peng and Li [16], and using an inverse algorithm based on conjugate gradient

* Corresponding author. Tel.: +98-233-230-0258; fax: +98-233-230-0258; e-mail: mghannadk@shahroodut.ac.ir

method and the discrepancy principle by Chang et al. [17], respectively. A thermostatic analysis of FG cylinders which were under uniform internal heat generation was conducted by Aziz and Torabi [18]. Xin et al. [19] presented a one-dimensional thermo-elasticity solution based on the volume fraction of constituents for FG cylinders under thermal and mechanical loading. In this study, the effects of volume fraction, thermal expansion coefficients and the ratio of two thermal expansion coefficients on displacement and stresses were systematically studied. Ghannd and Parhizkar Yaghoobi [20-21] presented the two-dimensional analysis (radial and axial direction of the cylinder) of thermo-elastic for homogeneous and FG cylinders under different boundary conditions (different mechanical and thermal conditions of the two ends of the cylinder).

Daneshmehr et al. [22] investigated the size-dependent free vibration of FGM Nano plates based on the nonlocal elasticity theory with high order theories. Using the higher order shear deformation theory (HSDT) and applying the principle of minimum potential energy, governing equations are obtained. In this research, the impacts of different parameters on the size-dependent frequency were discussed. The bending analysis and free vibration analysis of bi-directional Euler–Bernoulli nano-beams was performed by Zamani Nejad and Hadi [23-24]. Based on the Eringen's nonlocal elasticity theory, the equilibrium equation is derived and the generalized differential quadrature method (GDQM) is used to solve the governing equation. The effects of material length scale parameter and inhomogeneity constant on the bending analysis are studied. Moreover, the buckling analysis of arbitrary two-directional Euler–Bernoulli FGM nano-beams based on the nonlocal elasticity theory was done by Zamani Nejad et al. [25]. The influence of importance parameters on the buckling behavior of nano beams was investigated.

The FGM concept wasn't limited to application for conventional materials. There are many applications where the FGM concept is composed with smart materials or piezoelectric [26]. That explains why there are various types of methods currently available for analysis functionally graded piezoelectric material (FGPM), which mainly focus elasticity theories, shear deformation theory, simplified theories and mixed theories [26-32]. For example, the electro-thermo-elastic analysis of thick wall FGPM cylinders using the plane elasticity theory (PET) [27-29] and the asymmetric electro-thermo-elastic analysis of long piezoelectric FG cylinders [30-32] represent multiple physical analyses carried out on FGPM cylinders.

Zamani Nejad et al. [33] analyzed the free vibration behavior of arbitrary bi-directional Euler–Bernoulli nano-beams based on consistent couple-stress. The governing equation was extracted using energy method and solved by GDQM. The effects of various parameters on natural frequency were presented. Buckling and free vibration analysis of three-directional functionally graded material (TDFGM) Euler–Bernoulli nano-beam were done by Hadi et al. [34-35]. Except for Poisson's ratio, the material properties are assumed to be graded in all three directions, which may vary according to an arbitrary function. The governing equations were solved by employing GDQM and the parameters' effects were studied. Approximate analytical solutions to the bending analysis of the bi-directional FGM nano-beam are derived by using the Rayleigh-Ritz method [36]. The impact of changes to some important parameters on the values of deflection of nano-beam are studied. Ghaffari et al. [37] investigated the complete mechanical behavior analysis of FG Nano beam under non-uniform loading. The governing equations are derived by using the energy method and solved as a classical eigenvalue problem. The impact of size, non-homogeneity and non-uniform loads on bending, buckling and vibration behaviors is discussed.

Zarehzadeh et al. [38] performed a free torsional vibration analysis of FG nano-rod under magnetic field supported by a a generalized torsional foundation based on the nonlocal elasticity theory. The torque effect of an axial magnetic field on an FG nano-rod has been defined using Maxwell's relation and the governing equation was extracted by the Hamilton's principle. The problem was solved by GDQM and the results showed that an FG nano-rod model based on the nonlocal elasticity theory behaves more softly and has a smaller natural frequency. A static torsional analysis of bi-directional FG microtube based on the couple stress theory under magnetic field was presented by Barati et al. [39]. The Navier equation and boundary conditions of problem were derived by the minimum potential energy. The equations were solved by employing GDQM. The small-scale effect and heterogeneity constants on the static torsion were discussed. Dehshahri et al. [40] investigated free vibrations analysis of arbitrary three-dimensionally FGM nanoplates based on the modified strain gradient theory. The motion equations and boundary conditions of nanoplate are obtained using the Hamilton's principle and they were solved by GDQM. The effects of important parameters were studied. Barati et al. [41] analyzed the free vibration of bi-directional FG nanobeams subjected to magnetic field based on the nonlocal elasticity theory. The governing equation was obtained using energy method and solved by employing GDQM. The effects of the main parameters on vibrational behavior were investigated. Noroozi et al. [42] performed a free torsional vibration analysis of bi-directional FG nano-cone based on nonlocal strain gradient elasticity. The Navier equation and boundary conditions of the size-dependent nano-cone were derived by Hamilton's principle. The problem was solved by GDQM and the effects of some parameters, such as inhomogeneity constant, cross-sectional area parameter and small-scale parameters, were studied.

To the best of the researchers' knowledge, in the literature, no study has so far been carried out about the analytical solution of temperature distribution and thermal strain analysis in the cylinders with varying thickness and temperature-dependent material properties. As stated before, FGMs are commonly loaded with heat and work at high temperatures that are needed for analysis. Therefore, the current research can be considered as innovative and novel. In the present study, the heat conduction equation has been solved in cylinders with variable thickness, which are under thermal loading or thermal flux at their surfaces. The application of this research can be found in the analysis of cylinder structures with variable thickness whose surfaces are heated or cooled by fluids. Cooling towers or cooling blades are cases in point.. In this research, for the first time, using first-order temperature theory (FTT) and applying the virtual work method, the governing equations of FG cylinders with varying thickness that are subject to heat fluxes in their inner and outer layers are extracted with temperature-dependent properties. The governing equations are a set of nonlinear differential equations with variable coefficients whose solution is provided by the analytical method of matched asymptotic expansion of the perturbation technique. The proposed solution is highly accurate and its convergence is very fast. In this study, the effects of heterogeneity and temperature-dependency properties of cylinder with varying thickness are studied. The, research findings can be used to find optimum designed pressure vessels operating in high temperature circumstances. Also, the results of the present study are compared

with the results of the previous study, and a good agreement is observed.

2. Governing equations

Considering cylinder with varying thickness which has axisymmetric feature in terms of all features, one can ignore changes in the circumferential direction; therefore, the temperature distribution function in the cylinder is only a function of radius r and axis x. Moreover, it should be noted that in the proposed method, the surfaces of the cylinder are loaded under thermal flux. Therefore, when the fluid is in contact with the cylinder surfaces, it should not change the phase (not boiling or condensing). Therefore, for the temperature field, we have as follows:

$$T = T(r, x) \tag{1}$$

T is the temperature in the cylinder with varying thickness where $T(r, x)$ is a function of radius and axis of the cylinder.

A cylinder with varying thickness is made of FGM in this research is modeled as a power function such as [43-46], and the heterogeneity modeling of properties is studied using equation 2.

$$Pr(r) = Pr_i\left(\frac{r}{r_i}\right)^{n_{Pr}} = Pr_i\,\bar{r}^{\,n_{Pr}};\ \frac{r}{r_i} = \bar{r} \tag{2}$$

In equation 2, r_i is the inner radius of the cylinder and Pr_i indicates the properties of material in the inner layer of the cylinder, which could be mechanical and thermal properties such as the elasticity module, density, thermal expansion coefficient, thermal conductivity coefficient, etc. n_{Pr} in Eq. 2 is the heterogeneity constant; and the heterogeneity constant could be a positive or negative real number. Meantime, n_{Pr} = 0 shows homogenous materials.

Furthermore, the material properties in the inner layer of the FGM cylinder, which may be temperature-dependent, are expressed as a polynomial function of temperature (T) [47].

$$Pr_i(T) = Pr\left(P_{0i} + P_{1i}\,T + P_{2i}\,T^2 + P_{3i}\,T^3\right) \tag{3}$$

Where Pr and P_{ji} (j=0, 1, 2, 3) are material constants and subscript i represents a constituent of FGM.

In order to use the FTT, based on figure 1 the distance of each point from the cylinder with varying thickness to its symmetry axis r is expressed as its distance to the middle-layer of cylinder z plus middle-layer distance to the symmetry axis of cylinder R [20-21].

Based on what was said, we have:

$$\begin{aligned} r(x) &= R(x) + z \\ r_o(x) &= \frac{h_b - h_a}{L_C}x + h_a + r_i \\ R(x) &= \frac{r_o(x) + r_i}{2} = \frac{h_b - h_a}{2L_C}x + \frac{h_a}{2} + r_i \\ h(x) &= r_o(x) - r_i = \frac{h_b - h_a}{L_C}x + h_a \end{aligned} \tag{4}$$

and for the variation range of z and x, we have:

$$\begin{aligned} -\frac{h(x)}{2} \le z \le -\frac{h(x)}{2} \\ 0 \le x \le L_C \end{aligned} \tag{5}$$

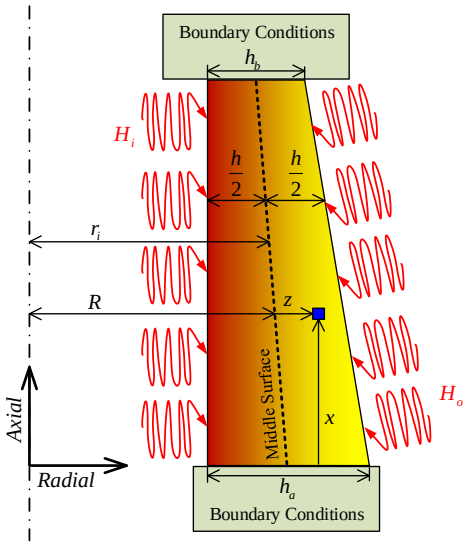

Figure 1. Cross-section of FGM cylinder with varying thickness subjected to heat fluxes at inner surface and outer surface.

The temperature field for cylinder with varying thickness using the FTT is expressed as follows [20-21]:

$$\begin{aligned} T = T(z,x) = T(0,x) + z\left.\frac{\partial T(z,x)}{\partial z}\right|_{z=0} + \frac{z^2}{2!}\left.\frac{\partial^2 T(z,x)}{\partial z^2}\right|_{z=0} \\ + \cdots = T^0(x) + z \times T^1(x) = T^0 + z \times T^1 \end{aligned} \tag{6}$$

Considering FTT in the Eq. 6, T^0 and T^1 are the zero-order and first-order components of temperature respectively, which are only a function of axial direction x. Considering T_R as the reference temperature, for temperature changes from the reference temperature $\Theta(z, x)$, we have:

$$\Theta(z,x) = T - T_R = \Theta^0(x) + z \times \Theta^1(x) = \Theta^0 + z \times \Theta^1 \tag{7}$$

Where Θ^0 and Θ^1 are the zero-order and first-order components of temperature change from the reference temperature. These functions are only a function of axial direction x. Using gradients relations (relation between temperature and thermal field) in the cylinder coordination [21, 48] and using Eq. 7, the thermal field-temperature changes relationships are derived.

$$\begin{aligned} e_z &= -\frac{\partial \Theta(x,z)}{\partial z} = -\Theta^1(x) \\ e_\theta &= 0 \\ e_x &= -\frac{\partial \Theta(x,z)}{\partial x} = -\frac{\mathrm{d}\Theta^0(x)}{\mathrm{d}x} - z\frac{\mathrm{d}\Theta^1(x)}{\mathrm{d}x} \end{aligned} \tag{8}$$

e_z, e_θ and e_x are thermal field components in the radial, circumferential, and axial directions. Also, the thermal strain [21] and heat flux [48] in the FGM cylinder with varying thickness are calculated as follows:

$$\varepsilon_i^t = \alpha\,\Theta; i = z, \theta, x \tag{9}$$

$$\begin{bmatrix} h_z \\ h_x \end{bmatrix} = \begin{bmatrix} k & 0 \\ 0 & k \end{bmatrix} \begin{bmatrix} e_z \\ e_x \end{bmatrix} \tag{10}$$

Where ε_i^T and h_i are the thermal strain and heat flux components in the radial (z), circumferential (θ), and axial (x) direction. Also, k is the thermal conduction coefficient and α is the thermal expansion coefficient in the said equation.

The material properties are described in a power function based on Eq. 2 and temperature-dependent based on Eq. 3, therefore we have [43-47]:

$$\begin{aligned} &k = k_i(T)\left(\frac{h_b - h_a}{2L_C r_i}x + \frac{h_a}{2r_i} + 1 + \frac{z}{r_i}\right)^n; \\ &k_i(T) = k\left(P_{0k} + P_{1k}T + P_{2k}T^2 + P_{3k}T^3\right) \\ &\alpha = \alpha_i(T)\left(\frac{h_b - h_a}{2L_C r_i}x + \frac{h_a}{2r_i} + 1 + \frac{z}{r_i}\right)^n; \\ &\alpha_i(T) = \alpha\left(P_{0\alpha} + P_{1\alpha}T + P_{2\alpha}T^2 + P_{3\alpha}T^3\right) \end{aligned} \tag{11}$$

The heterogeneity of properties in the FGM cylinder with varying thickness is a function of the two variables of (z) and (x). $k_i(T)$ is the value of thermal conductivity coefficient, $\alpha_i(T)$ is the coefficient of thermal expansion in the inner layer of the cylinder with varying thickness and n is the heterogeneity constant. Also, figure 2 shows the inner and outer surfaces of FG cylinder is subjected to heat flux H_i and H_o, respectively.

The thermal results are defined as follows [20-21]:

$$\begin{aligned} &\begin{Bmatrix} N_z^t \\ N_x^t \end{Bmatrix} = \int_{-h/2}^{h/2} \begin{Bmatrix} h_z \\ h_x \end{Bmatrix} \left(1 + \frac{z}{R(x)}\right) \mathrm{d}z \\ &M_x^t = \int_{-h/2}^{h/2} h_x \left(1 + \frac{z}{R(x)}\right) z \, \mathrm{d}z \end{aligned} \tag{12}$$

Based on the principle of virtual work, the variations of the structure potential energy are equal to work variations due to external forces $\delta W = \delta U$ [20-21] where U is the thermal potential energy of the whole body and W is the total work due to the applied heat flux in the inner and outer surfaces of the cylinder. The thermal potential energy of the entire body and the work resulting from these heat fluxes are calculated as follows:

$$\begin{cases} U = \iiint U^* \, \mathrm{d}\Omega; \mathrm{d}\Omega = r\mathrm{d}r\mathrm{d}\theta\mathrm{d}x = (R(x) + z)\mathrm{d}z\mathrm{d}\theta\mathrm{d}x \\ U^* = -\frac{1}{2}\left(h_z e_z + h_x e_x\right) \end{cases} \tag{13}$$

$$W = -\iint_S \left(H_i \Theta\big|_{r=r_i} + H_o \Theta\big|_{r=r_o(x)}\right) \mathrm{d}S \tag{14}$$

$$\begin{aligned} &\delta U = -\int_0^{L_C} \int_0^{2\pi} \int_{-\frac{h}{2}}^{-\frac{h}{2}} \left(h_z \delta e_z + h_x \delta e_x\right)(R(x) + z)\,\mathrm{d}z\mathrm{d}\theta\mathrm{d}x \\ &\delta W = -\int_0^{L_C} \int_0^{2\pi} \left(H_i \, \delta\Theta\big|_{r=r_i} (R(x) - \frac{h(x)}{2}) \right. \\ &\left. + H_o \, \delta\Theta\big|_{r=r_o(x)} (R(x) + \frac{h(x)}{2})\right) \mathrm{d}\theta\mathrm{d}x \end{aligned} \tag{15}$$

By inserting Eqs. 7-8 in Eq. 15, using the virtual work principle and performing mathematical operation and simplification, the governing equations are obtained as follows:

$$\begin{cases} \dfrac{\mathrm{d}(R(x)N_x^t)}{\mathrm{d}x} = H_i\left(R(x) - \dfrac{h(x)}{2}\right) \\ + H_o\left(R(x) + \dfrac{h(x)}{2}\right) \\ R(x)N_z^t - \dfrac{\mathrm{d}(R(x)M_x^t)}{\mathrm{d}x} = \dfrac{h(x)}{2}\left(H_i\left(R(x) - \dfrac{h(x)}{2}\right)\right) \\ - \dfrac{h(x)}{2}\left(H_o\left(R(x) + \dfrac{h(x)}{2}\right)\right) \end{cases} \tag{16}$$

$$\begin{cases} R(x)N_x^t \delta\Theta^0\big|_{x=0,L_C} = 0 \\ R(x)M_x^t \delta\Theta^1\big|_{x=0,L_C} = 0 \end{cases} \tag{17}$$

For simplifying, the first equation of system Eq. 16 is integrated and we have:

$$\begin{cases} R(x)N_x^t = \int\left(H_i\left(R(x) - \dfrac{h(x)}{2}\right)\right. \\ \left. + H_o\left(R(x) + \dfrac{h(x)}{2}\right)\right)\mathrm{d}x + K1 \\ R(x)N_z^t - \dfrac{\mathrm{d}(R(x)M_x^t)}{\mathrm{d}x} = \dfrac{h(x)}{2}\left(H_i\left(R(x) - \dfrac{h(x)}{2}\right)\right) \\ - \dfrac{h(x)}{2}\left(H_o\left(R(x) + \dfrac{h(x)}{2}\right)\right) \end{cases} \tag{18}$$

Where K_1 is the constant of integrating operation from the first equation of system Eq. 16. This equation could be shown in the short form as follows:

$$\begin{cases} N_x^t + F1(x) = 0; \\ F1(x) = \left(\dfrac{-1}{R(x)}\right)\left(\int H_i\left(R(x) - \dfrac{h(x)}{2}\right)\right. \\ \left. + H_o\left(R(x) + \dfrac{h(x)}{2}\right)\mathrm{d}x + K1\right) \\ R(x)N_z^t - \dfrac{\mathrm{d}(R(x)M_x^t)}{\mathrm{d}x} + F2(x) = 0; \\ F2(x) = \dfrac{h(x)}{2}\left(H_o\left(R(x) + \dfrac{h(x)}{2}\right) - H_i\left(R(x) - \dfrac{h(x)}{2}\right)\right) \end{cases} \tag{19}$$

By inserting Eqs. 7-12 in Eq. 19, the equation system is obtained in terms of zero-order and first-order components of the temperature variation (Θ^0 and Θ^1). This equation system, which is a nonlinear ordinary differential equation with variable coefficients, is in the general form as follows by assuming n=1, and its dimensionless form will be reported.

$$\begin{cases} L_1\Big[x,\dfrac{\mathrm{d}}{\mathrm{d}x},\Theta^0\dfrac{\mathrm{d}}{\mathrm{d}x},\Theta^1\dfrac{\mathrm{d}}{\mathrm{d}x},\Theta^{0^2}\dfrac{\mathrm{d}}{\mathrm{d}x},\Theta^{1^2}\dfrac{\mathrm{d}}{\mathrm{d}x},\Theta^{0^3}\dfrac{\mathrm{d}}{\mathrm{d}x},\Theta^{1^3}\dfrac{\mathrm{d}}{\mathrm{d}x},\\ \Theta^0,\Theta^1,\Theta^{0^2},\Theta^{1^2},\Theta^{0^3},\Theta^{1^3},F1,R,h,k,P_{0k},P_{1k},P_{2k},P_{3k}\Big]=0\\ L_2\Big[x,\dfrac{\mathrm{d}}{\mathrm{d}x},\dfrac{\mathrm{d}^2}{\mathrm{d}x^2},\Theta^0\dfrac{\mathrm{d}}{\mathrm{d}x},\Theta^1\dfrac{\mathrm{d}}{\mathrm{d}x},\Theta^{0^2}\dfrac{\mathrm{d}}{\mathrm{d}x},\Theta^{1^2}\dfrac{\mathrm{d}}{\mathrm{d}x},\Theta^{0^3}\dfrac{\mathrm{d}}{\mathrm{d}x},\\ \Theta^{1^3}\dfrac{\mathrm{d}}{\mathrm{d}x},\left(\dfrac{\mathrm{d}}{\mathrm{d}x}\right)^2,\Theta^0\left(\dfrac{\mathrm{d}}{\mathrm{d}x}\right)^2,\Theta^1\left(\dfrac{\mathrm{d}}{\mathrm{d}x}\right)^2,\Theta^{0^2}\left(\dfrac{\mathrm{d}}{\mathrm{d}x}\right)^2,\\ \Theta^{1^2}\left(\dfrac{\mathrm{d}}{\mathrm{d}x}\right)^2,\Theta^1\dfrac{\mathrm{d}^2}{\mathrm{d}x^2},\Theta^0\dfrac{\mathrm{d}^2}{\mathrm{d}x^2},\Theta^{0^2}\dfrac{\mathrm{d}^2}{\mathrm{d}x^2},\Theta^{1^2}\dfrac{\mathrm{d}^2}{\mathrm{d}x^2},\Theta^{0^3}\dfrac{\mathrm{d}^2}{\mathrm{d}x^2},\\ \Theta^{1^3}\dfrac{\mathrm{d}^2}{\mathrm{d}x^2},\Theta^0,\Theta^1,\Theta^{0^2},\Theta^{1^2},\Theta^{0^3},\Theta^{1^3},\Theta^{1^4},\\ F2,R,h,k,P_{0k},P_{1k},P_{2k},P_{3k}\Big]=0 \end{cases} \tag{20}$$

Where L_1 and L_2 are differential operators.

3. Analytical Solution

In order to solve the governing Eq. 20, in this study, the matched asymptotic expansion method of perturbation technique is used. For this purpose, it is necessary first to make the governing equation system dimensionless. The governing equations system is made dimensionless by using the parameters defined below.

$$\begin{cases} x^*=\dfrac{x}{L_C};\ h^*=\dfrac{h}{h_0};\ R^*=\dfrac{R}{h_0};\ k^*=\dfrac{k}{k}=1;P_{0k}^*=P_{0k};\\ P_{1k}^*=\dfrac{P_{1k}}{\alpha};P_{2k}^*=\dfrac{P_{2k}}{\alpha^2};P_{3k}^*=\dfrac{P_{3k}}{\alpha^3};\varepsilon=\dfrac{h_0}{L_C};\Theta^{0*}=\Theta^0\alpha;\\ \psi=\dfrac{2R+h}{2R-h};\varsigma^*=\varepsilon\times\dfrac{\mathrm{d}\Theta^{0*}}{\mathrm{d}x^*};m^*=\ln(\dfrac{2R+h}{2R-h});T_R^*=T_R\alpha;\\ \Theta^{1*}=\Theta^1h_0\,\alpha;\ F2^*=F2\times\dfrac{\varepsilon\,\alpha}{\varepsilon_1h_0\,k};\ F1^*=F1\times\dfrac{\varepsilon\,\alpha}{\varepsilon_1k}; \end{cases} \tag{21}$$

Where h_0 is the index thickness and ε is a small parameter. The presence of the star sign on the parameters indicates dimensionless quantities. In this research, ε is selected as a perturbation parameter and ε_1 is magnitude of the perturbation parameter. Using the dimensionless parameters (21), a dimensionless form of the Eq. 20 is obtained.

In order to reduce the writing volume of dimensionless governing equations, the heterogeneity constant is assumed to equal one and reference temperature is zero (n =0 & T_R=0). Therefore, the system of governing equations, made dimensionless with n =0 & T_R=0, is obtained as follows:

$$\begin{aligned} &O(\varepsilon^4)+O(\varepsilon^3)+O(\varepsilon^2)-\Big[20k^*\frac{\mathrm{d}\Theta^{1*}}{\mathrm{d}x^*}h^{*3}P_{0k}^*\\ &+3P_{2k}^*k^*\Theta^{1*^2}\frac{\mathrm{d}\Theta^{1*}}{\mathrm{d}x^*}h^{*5}+20P_{1k}^*k^*\Theta^{1*}R^*\frac{\mathrm{d}\Theta^{1*}}{\mathrm{d}x^*}h^{*3}\\ &-\frac{240F1^*R^*}{\varepsilon_1}+40k^*h^{*3}P_{2k}^*\varsigma^*\Theta^{0*}\Theta^{1*}\\ &+240k^*h^*\varsigma^*R^*P_{2k}^*\Theta^{0*^2}+3k^*h^{*5}\Theta^{1*^3}P_{3k}^*R^*\frac{\mathrm{d}\Theta^{1*}}{\mathrm{d}x^*}\\ &+60k^*h^{*3}\Theta^{1*^2}\varsigma^*R^*P_{3k}^*\Theta^{0*}\Big]\varepsilon-3k^*h^{*5}\Theta^{1*^3}P_{3k}^*\varsigma^*\\ &-20k^*h^{*3}\varsigma^*P_{1k}^*\Theta^{1*}-20k^*h^{*3}\Theta^{1*^2}\varsigma^*R^*P_{2k}^*=0 \end{aligned} \tag{22a}$$

$$\begin{aligned} &O(\varepsilon^5)+O(\varepsilon^4)+O(\varepsilon^3)+O(\varepsilon^2)+\Big[560k^*h^{*3}\frac{\mathrm{d}\varsigma^*}{\mathrm{d}x^*}P_{0k}^*\varepsilon_1\\ &-1680k^*\Theta^{1*^3}h^{*5}R^*P_{2k}^*\Theta^{0*}\varepsilon_1\\ &-6720k^*\Theta^{1*}h^*R^*P_{1k}^*\Theta^{0*}\varepsilon_1\\ &+84k^*h^{*5}R^*\Theta^{1*^3}P_{3k}^*\frac{\mathrm{d}\varsigma^*}{\mathrm{d}x^*}\varepsilon_1\\ &+1120k^*h^{*3}R^*\frac{\mathrm{d}\Theta^{1*}}{\mathrm{d}x^*}P_{1k}^*\varsigma^*\varepsilon_1\\ &560k^*h^{*3}R^*\Theta^{1*}\frac{\mathrm{d}\varsigma^*}{\mathrm{d}x^*}P_{1k}^*\varepsilon_1+1120k^*h^{*3}\varsigma^{*2}P_{2k}^*\Theta^{0*}\varepsilon_1\\ &+336k^*h^{*5}\Theta^{1*}\frac{\mathrm{d}\Theta^{1*}}{\mathrm{d}x^*}P_{2k}^*\varsigma^*\varepsilon_1\\ &+3360k^*h^{*3}R^*\Theta^{1*}\varsigma^{*2}P_{3k}^*\varsigma^*\Theta^{0*}\varepsilon_1\\ &+504k^*h^{*5}R^*\Theta^{1*^2}\frac{\mathrm{d}\Theta^{1*}}{\mathrm{d}x^*}P_{3k}^*\varsigma^*\varepsilon_1\\ &-1120k^*\Theta^{1*^2}h^{*3}P_{2k}^*\Theta^{0*}\varepsilon_1\\ &+6720F2^*+84k^*h^{*5}\Theta^{1*^2}\frac{\mathrm{d}\varsigma^*}{\mathrm{d}x^*}P_{2k}^*\varepsilon_1\Big]\varepsilon\\ &-6720k^*\Theta^{1*}h^*R^*P_{0k}^*\varepsilon_1-560k^*\Theta^{1*^3}h^{*3}R^*P_{2k}^*\varepsilon_1\\ &+252k^*h^{*5}\Theta^{1*^2}\varsigma^{*2}P_{3k}^*\varepsilon_1+560k^*h^{*3}\varsigma^{*2}P_{1k}^*\varepsilon_1\\ &-84k^*\Theta^{1*^4}h^{*5}P_{3k}^*\varepsilon_1-560k^*\Theta^{1*^2}h^{*3}P_{1k}^*\varepsilon_1\\ &+1120k^*h^{*3}R^*\Theta^{1*}\varsigma^{*2}P_{2k}^*\varepsilon_1=0 \end{aligned} \tag{22b}$$

Differential Eqs 22a-22b are second-order differential equations whose order is reduced by twice by equaling perturbation term to zero ($\varepsilon=0$) and become an algebraic equation. Based on the theory of perturbations, it shows that there are two boundary layers in the two cylinder's heads. In other words, solving the problem involves two sections; one is the outer solution in regions located far from the boundaries, and the other is the inner solution in the boundaries or the shell's two head regions [49-50].

As noted earlier, in order to facilitate and reduce the written volume of dimensionless equations, a heterogeneity constant and reference temperature equal to zero were taken into consideration (n =0 & T_R=0). For other heterogeneity constant and reference temperature values, the solution procedure is the same and the dimensionless equations should be derived based on the heterogeneity constant and reference temperature values. Then, the process of outer and inner solution is studied in light of dimensionless governing equations with heterogeneity constant and reference temperature equaling zero (Eqs. 22a-22b).

3.1. Outer Solution

The outer solution is considered as a uniform series of perturbation term (ε). By substituting this uniform series in Eqs. 22a-22b, and considering the dominant sentences, this series (inner solution) is expressed as follows:

$$\begin{cases} Y_{outer}=Y_0+\varepsilon Y_1\\ Y_0=\begin{bmatrix}\varsigma_0(x^*)\\ \Theta_0^1(x^*)\end{bmatrix};\ Y_1=\begin{bmatrix}\varsigma_1(x^*)\\ \Theta_1^1(x^*)\end{bmatrix} \end{cases} \tag{23}$$

By substituting Eq. 22 with Eq. 23 and considering the coefficients of ε^0 and ε^1, the algebraic equations relating to the zero-order and first-order outer solution can be achieved as follows:

$$O(\varepsilon^0)\rightarrow\begin{cases} k*h*P_{0k}^{*}\varepsilon_1\varsigma_0 - F1^{*}=0 \\ \\ k*h*R*P_{0k}^{*}\varepsilon_1\Theta_0^1 - F2^{*}=0 \end{cases} \tag{24a}$$

$$O(\varepsilon^1)\rightarrow\begin{cases} h^{*2}P_{0k}^{*}\dfrac{\mathrm{d}\Theta_0^1}{\mathrm{d}x^{*}} + h^{*2}P_{1k}^{*}\varsigma_0\Theta_0^1 + 12P_{0k}^{*}R^{*}\varsigma_1 = 0 \\ \\ h^{*2}P_{0k}^{*}\dfrac{\mathrm{d}\varsigma_0}{\mathrm{d}x^{*}} + h^{*2}P_{1k}^{*}{\varsigma_0}^2 - h^{*2}P_{1k}^{*}{\Theta_0^1}^2 \\ -12R^{*}P_{0k}^{*}\Theta_1^1 = 0 \end{cases} \tag{24b}$$

Eqs. 24a-24b are the linear algebraic equations relating to zero-order and first-order outer solutions respectively, which are easily solved to determine the zero-order outer solution (Y_0) and first-order outer solution (Y_1).

3.2 Inner Solution in the cylinder's lower boundary ($x^{*}=0$)

Based on the matched asymptotic expansion perturbation technique for the solution in the boundary regions, the fast variable should be used. For the inner solution in the boundary regions near the bottom of cylinder, $\eta = x^{*}/\varepsilon$ is selected as the fast variable and the Taylor expansion is written for loading, thickness, middle-layer radius in the lower boundary regions ($x^{*}=0$) . Therefore, we have:

$$\begin{cases} R^{*}(x^{*}) = {R_0}^{*} + \varepsilon\eta\,\mathrm{d}R_0 + \cdots; \\ {R_0}^{*} = R^{*}(0),\ \mathrm{d}R_0 = \left.\dfrac{\mathrm{d}R^{*}}{\mathrm{d}x^{*}}\right|_{x^{*}=0} \\ h^{*}(x^{*}) = {h_0}^{*} + \varepsilon\eta\,\mathrm{d}h_0 + \cdots; \\ {h_0}^{*} = h^{*}(0),\ \mathrm{d}h_0 = \left.\dfrac{\mathrm{d}h^{*}}{\mathrm{d}x^{*}}\right|_{x^{*}=0} \\ F1^{*}(x^{*}) = {F1_0}^{*} + \varepsilon\eta\,\mathrm{d}F1_0 + \cdots; \\ {F1_0}^{*} = F1^{*}(0),\ \mathrm{d}F1_0 = \left.\dfrac{\mathrm{d}F1^{*}}{\mathrm{d}x^{*}}\right|_{x^{*}=0} \\ F2^{*}(x^{*}) = {F2_0}^{*}(0) + \varepsilon\eta\,\mathrm{d}F2_0 + \cdots; \\ {F2_0}^{*} = F2^{*}(0),\ \mathrm{d}F2_0 = \left.\dfrac{\mathrm{d}F2^{*}}{\mathrm{d}x^{*}}\right|_{x^{*}=0} \end{cases} \tag{25}$$

The inner solution is assumed as follows:

$$\begin{cases} Y_{inner} = Y_{0i} + \varepsilon Y_{1i} \\ Y_{0i} = \begin{bmatrix} \varsigma_{0i}(\eta) \\ \Theta_{0i}^1(\eta) \end{bmatrix};\ Y_{1i} = \begin{bmatrix} \varsigma_{1i}(\eta) \\ \Theta_{1i}^1(\eta) \end{bmatrix} \end{cases} \tag{26}$$

By substituting Eq. 22 with Eqs. 25-26 and taking into considering the coefficients of ε^0 and ε^1, the differential equation system related to the zero-order and first-order inner solution are achieved for the lower boundary.

$$O(\varepsilon^0)\rightarrow\begin{cases} L_{2i}[Y_{0i}] + \{F0i\} = 0; \\ L_{2i}[\bullet] = [D2i]\dfrac{\mathrm{d}^2\{\bullet\}}{\mathrm{d}\eta^2} + [D1i]\dfrac{\mathrm{d}\{\bullet\}}{\mathrm{d}\eta} + [D0i]\{\bullet\} \\ [D2i] = \begin{bmatrix} 0 & 0 \\ 0 & D2i_{22} \end{bmatrix},[D1i] = \begin{bmatrix} 0 & D1i_{12} \\ D1i_{21} & 0 \end{bmatrix}, \\ [D0i] = \begin{bmatrix} D0i_{11} & 0 \\ 0 & D0i_{22} \end{bmatrix} \\ \{F0i\} = \begin{Bmatrix} F0i_1 \\ F0i_2 \end{Bmatrix} \end{cases} \tag{27a}$$

$$O(\varepsilon^1)\rightarrow\begin{cases} L_{2i}[Y_{1i}] + \{F1i\} = 0; \\ \{F1i\} = \begin{Bmatrix} F1i_1 \\ F1i_2 \end{Bmatrix} \end{cases} \tag{27b}$$

Where $[D2i]_{2\times2}$, $[D1i]_{2\times2}$, and $[D0i]_{2\times2}$ are the coefficients matrices, $\{F0i\}$ and $\{F1i\}$are the vectors (nonhomogeneous part of differential equation system). Non-zero components of these matrices and vectors are as follows:

$$\begin{cases} D2i_{22} = 560k*P_{0k}^{*}\varepsilon_1{h_0}^{*3}{R_0}^{*};\ D1i_{12} = -20k*{h_0}^{*3}P_{0k}^{*}\varepsilon_1; \\ D1i_{21} = 560k*P_{0k}^{*}\varepsilon_1{h_0}^{*3};\ D0i_{11} = -240k*h_0*P_{0k}^{*}\varepsilon_1{R_0}^{*}; \\ D0i_{22} = -6720k*P_{0k}^{*}\varepsilon_1h_0*{R_0}^{*}; \\ F0i_1 = 240F1_0*{R_0}^{*};\ F0i_2 = 6720F2_0^{*}; \\ F1i_1 = -240k*P_{0k}^{*}\eta\mathrm{d}h_0R_0*\varepsilon_1\varsigma_{0i}(\eta) \\ -20k*{h_0}^{*3}P_{0k}^{*}\varepsilon_1R_0*\Theta_{0i}^1(\eta)\dfrac{\mathrm{d}\Theta_{0i}^1(\eta)}{\mathrm{d}\eta} \\ -240k*P_{0k}^{*}h_0*\eta\,\mathrm{d}R_0\,\varepsilon_1\varsigma_{0i}(\eta) + 240F1_0*\mathrm{d}R_0 \\ -60k*P_{0k}^{*}{h_0}^{*2}\eta\mathrm{d}h_0\varepsilon_1\dfrac{\mathrm{d}\Theta_{0i}^1(\eta)}{\mathrm{d}\eta} \\ -20k*{h_0}^{*3}\varepsilon_1P_{0k}^{*}\varsigma_{0i}(\eta)\Theta_{0i}^1(\eta) - 20k*{h_0}^{*3}\varepsilon_1P_{0k}^{*}; \\ F1i_2 = -6720k*P_{0k}^{*}\varepsilon_1h_0*{R_0}^{*}\Theta_{0i}^1(\eta) \\ +560k*P_{0k}^{*}\varepsilon_1{h_0}^{*3}\dfrac{\mathrm{d}^2\Theta_{0i}^1(\eta)}{\mathrm{d}\eta^2} + 6720F2_0* \\ +1680k*P_{0k}^{*}{h_0}^{*2}\eta\mathrm{d}h_0\varepsilon_1\dfrac{\mathrm{d}\varsigma_{0i}(\eta)}{\mathrm{d}\eta} \\ +1120k*P_{1k}^{*}\varepsilon_1{h_0}^{*3}{R_0}^{*}\dfrac{\mathrm{d}\Theta_{0i}^1(\eta)}{\mathrm{d}\eta}\varsigma_{0i}(\eta) \\ +560k*P_{1k}^{*}\varepsilon_1{h_0}^{*3}{R_0}^{*}\Theta_{0i}^1(\eta)\dfrac{\mathrm{d}\varsigma_{0i}(\eta)}{\mathrm{d}\eta} \\ -6720\left(h_0*\mathrm{d}R_0 + \mathrm{d}h_0R_0^{*}\right)k*P_{0k}^{*}\varepsilon_1\eta\Theta_{0i}^1(\eta) \\ +\left(560{h_0}^{*3}\mathrm{d}R_0 + 1680{h_0}^{*2}\mathrm{d}h_0R_0^{*}\right)k*P_{0k}^{*}\varepsilon_1\eta\dfrac{\mathrm{d}^2\Theta_{0i}^1(\eta)}{\mathrm{d}\eta^2} \\ +k*P_{1k}^{*}\varepsilon_1\left(560{h_0}^{*3}\left(\varsigma_{0i}(\eta)\right)^2 + 84{h_0}^{*5}\Theta_{0i}^1(\eta)\dfrac{\mathrm{d}^2\Theta_{0i}^1(\eta)}{\mathrm{d}\eta^2}\right) \\ +84k*P_{1k}^{*}\varepsilon_1{h_0}^{*5}\left(\dfrac{\mathrm{d}\Theta_{0i}^1(\eta)}{\mathrm{d}\eta}\right)^2 - 560k*P_{1k}^{*}\varepsilon_1{h_0}^{*3}\left(\Theta_{0i}^1(\eta)\right)^2 \end{cases} \tag{28}$$

The general solution of Eqs. 27a-27b is $\{Y\}=\{V_i\}\,e^{\lambda_i\eta}$ where λ_i is the eigenvalue and $\{V_i\}$ is its eigenvector [21]. To achieve eigenvalues, we substitute the general solution in the homogenous equations of 27a and 27b. Considering that the homogenous part of Eqs. 27a-27b is identical the general solution of both equations of 27a and 27b is the same and we have:

$$[C]_{2\times2}\{V_i\}=\{0\};\quad [C]=\lambda_i^2[D2i]+\lambda_i[D1i]+[D0i] \tag{29}$$

In order to find the value of λ_i, Eq. 29 should have a non-evident answer ($\{V_i\}\neq\{0\}$). Therefore, by equaling the coefficients determinant to zero (det[C]=0), the characteristic equation is achieved, whose solution would produce the eigenvalues or the value of λ_i. This characteristic equation is an algebraic second-order equation whose solution would help determine two values for the eigenvalues. The corresponding vector for each eigenvalue is also calculated. Since the inner solution value should have a limited value in the region far from the lower boundary (positive infinity), the root should be chosen so that their real part would be negative and their value would be limited in infinity. So, an eigenvalue (having negative real value) and its corresponding vector are chosen and for the general solution, we have:

$$\{Y\}_g=C_1\{V_1\}e^{\lambda_1\eta} \tag{30}$$

The particular solution of Eqs. 27a and 27b considering their non-homogenous part is determined as $\{F0i\}$ and $\{F1i\}$, respectively. Considering that the non-homogenous part of Eq. 27a is a constant value, the particular solution for Eq. 27a is assumed as $\{Y\}_{p0}=\{K_0\}$ and the vector $\{K_0\}$ is determined by inserting the solution in Eq. 27a. The solution of Eq. 27a is achieved as $\{Y\}=\{Y\}_g+\{Y\}_{p0}$ where the constant C_1 in the solution is determined by applying boundary conditions relating to the last vector term $\{Y\}$ in $x^*=0$.

The non-homogenous part of Eq. 27b has two parts; one part includes polynomial terms and the other part includes exponential terms. Therefore, considering the non-homogenous part of Eq. 27b, the particular solution is assumed to have two parts. The polynomial part of the particular solution is $\{Y\}_{p11}=\{K_1\}\eta+\{K_0\}$. $\{K_0\}$ and $\{K_1\}$ are the constant vectors which are determined by substituting in Eq. 27b based on the polynomial term of non-homogenous part. Since the exponential terms of the non-homogenous part of Eq. 27b also includes the general solution, the exponential part of the particular solution is $\{Y\}_{p12}=(\{V_2\}\eta^2+\{V_1\}\eta+\{V_0\})\,e^{\lambda_1\eta}+\sum\{U_j\}\,e^{\beta_j\eta}$ where $\{V_0\}$, $\{V_1\}$, $\{V_2\}$ and $\{U_j\}$ are the constant vectors that they are determined by substituting in Eq. 27b based the exponential terms of non-homogenous part. The solution of Eq. 27b is $\{Y\}=\{Y\}_g+\{Y\}_{p11}+\{Y\}_{p12}$ in which the constant is achieved by applying the boundary condition related to the last vector term of $\{Y\}$ in $x^*=0$.

3.3 Inner Solution in cylinder's upper boundary ($x^*=1$)

Based on what was said in the last section, a fast variable is also used in the upper limit. For the inner solution in the boundary conditions near the top of cylinder, $\zeta=(x^*-1)/\varepsilon$ is used as the fast variable and the Taylor expansion for loading, thickness, middle-layer radius in the upper boundary regions ($x^*=1$) are written. Therefore, we have:

$$\begin{cases}
R^*(x^*)=R_1^*+\varepsilon\zeta\,\mathrm{d}R_1+\cdots;\\
R_1^*=R^*(1),\ \mathrm{d}R_1=\left.\dfrac{\mathrm{d}R^*}{\mathrm{d}x^*}\right|_{x^*=1}\\
h^*(x^*)=h_1^*+\varepsilon\zeta\,\mathrm{d}h_1+\cdots;\\
h_1^*=h^*(1),\ \mathrm{d}h_1=\left.\dfrac{\mathrm{d}h^*}{\mathrm{d}x^*}\right|_{x^*=1}\\
F1^*(x^*)=F1_1^*+\varepsilon\zeta\,\mathrm{d}F1_1+\cdots;\\
F1_1^*=F1^*(1),\ \mathrm{d}F1_1=\left.\dfrac{\mathrm{d}F1^*}{\mathrm{d}x^*}\right|_{x^*=1}\\
F2^*(x^*)=F2_1^*(0)+\varepsilon\zeta\,\mathrm{d}F2_1+\cdots;\\
F2_1^*=F2^*(1),\ \mathrm{d}F2_1=\left.\dfrac{\mathrm{d}F2^*}{\mathrm{d}x^*}\right|_{x^*=1}
\end{cases} \tag{31}$$

The inner solution is assumed as follows:

$$\begin{cases}
Y_{Inner}=Y_{0I}+\varepsilon Y_{1I}\\
Y_{0I}=\begin{bmatrix}\varsigma_{0I}(\zeta)\\ \Theta_{0I}^1(\zeta)\end{bmatrix};\quad Y_{1I}=\begin{bmatrix}\varsigma_{1I}(\zeta)\\ \Theta_{1I}^1(\zeta)\end{bmatrix}
\end{cases} \tag{32}$$

By substituting Eq. 22 with Eqs. 31-32 and taking into considering the coefficients of ε^0 and ε^1, the differential equation system related to the zero-order and first-order inner solution are achieved for the upper boundary.

$$O(\varepsilon^0)\rightarrow\begin{cases}
L_{2I}[Y_{0I}]+\{F0I\}=0;\\
L_{2I}[\bullet]=[D2I]\dfrac{\mathrm{d}^2\{\bullet\}}{\mathrm{d}\zeta^2}+[D1I]\dfrac{\mathrm{d}\{\bullet\}}{\mathrm{d}\zeta}+[D0I]\{\bullet\}\\
\{F0I\}=\begin{Bmatrix}F0I_1\\ F0I_2\end{Bmatrix}
\end{cases} \tag{33a}$$

$$O(\varepsilon^1)\rightarrow\begin{cases}
L_{2I}[Y_{1I}]+\{F1I\}=;\\
\{F1I\}=\begin{Bmatrix}F1I_1\\ F1I_2\end{Bmatrix}
\end{cases} \tag{33b}$$

Where $[D2I]_{2\times2}$, $[D1I]_{2\times2}$, and $[D0I]_{2\times2}$ are the coefficient matrices, $\{F0I\}$ and $\{F1I\}$ are the vectors (nonhomogeneous part of differential equation system). The non-zero components of these vectors and matrices are as follows:

$$\begin{cases}
D2I_{22}=560k*P_{0k}^*\varepsilon_1h_1{}^{*3}\,R_1^*;\ D1I_{12}=-20k*h_1{}^{*3}\,P_{0k}^*\varepsilon_1;\\
D1I_{21}=560k*P_{0k}^*\varepsilon_1h_1{}^{*3};\ D0I_{11}=-240k*h_1^*P_{0k}^*\varepsilon_1R_1^*;\\
D0I_{22}=-6720k*P_{0k}^*\varepsilon_1h_1^*R_1^*;\\
F0I_1=240F1_1^*R_1^*;\ F0I_2=6720F2_1^*;\\
F1I_1=-240k*P_{0k}^*\eta\,\mathrm{d}h_1R_1^*\varepsilon_1\varsigma_{0I}(\eta)\\
-20k*h_1{}^{*3}\,P_{0k}^*\varepsilon_1R_1^*\Theta_{0I}^1(\eta)\dfrac{\mathrm{d}\Theta_{0I}^1(\eta)}{\mathrm{d}\eta}\\
-240k*P_{0k}^*h_1^*\eta\,\mathrm{d}R_1\,\varepsilon_1\varsigma_{0I}(\eta)\\
-60k*P_{0k}^*h_1{}^{*2}\,\eta\mathrm{d}h_1\varepsilon_1\dfrac{\mathrm{d}\Theta_{0I}^1(\eta)}{\mathrm{d}\eta}\\
-20k*h_1{}^{*3}\,\varepsilon_1P_{0k}^*\varsigma_{0I}(\eta)\Theta_{0I}^1(\eta)\\
240F1_1^*\mathrm{d}R_1-20k*h_1{}^{*3}\,\varepsilon_1P_{0k}^*;
\end{cases} \tag{34}$$

$$
\begin{aligned}
&F1I_2 = -6720k*P_{0k}^{*}\varepsilon_1 h_1 * R_1 * \Theta_{0I}^{1}(\eta) \\
&+560k*P_{0k}^{*}\varepsilon_1 h_1{}^{*3}\frac{\mathrm{d}^2\Theta_{0I}^{1}(\eta)}{\mathrm{d}\eta^2} + 6720F2_I * \\
&+1680k*P_{0k}^{*}h_1{}^{*2}\,\eta \mathrm{d}h_1\varepsilon_1\frac{\mathrm{d}\varsigma_{0I}(\eta)}{\mathrm{d}\eta} \\
&+1120k*P_{1k}^{*}\varepsilon_1 h_I{}^{*3}R_I * \frac{\mathrm{d}\Theta_{0I}^{1}(\eta)}{\mathrm{d}\eta}\varsigma_{0I}(\eta) \\
&+560k*P_{1k}^{*}\varepsilon_1 h_1{}^{*3}R_1 * \Theta_{0I}^{1}(\eta)\frac{\mathrm{d}\varsigma_{0I}(\eta)}{\mathrm{d}\eta} \\
&-6720k*P_{0k}^{*}h_1 * \eta \mathrm{d}R_1\varepsilon_1\Theta_{0I}^{1}(\eta) \\
&-6720k*P_{0k}^{*}\eta \mathrm{d}h_1 R_1 * \varepsilon_1\Theta_{0I}^{1}(\eta) \\
&+560k*P_{0k}^{*}\varepsilon_1 h_1{}^{*3}\eta \mathrm{d}R_1\frac{\mathrm{d}^2\Theta_{0I}^{1}(\eta)}{\mathrm{d}\eta^2} \\
&+1680k*P_{0k}^{*}\varepsilon_1 h_1{}^{*2}\eta \mathrm{d}h_1 R_1 * \frac{\mathrm{d}^2\Theta_{0I}^{1}(\eta)}{\mathrm{d}\eta^2} \\
&+560k*P_{1k}^{*}\varepsilon_1 h_1{}^{*3}\left(\varsigma_{0I}(\eta)\right)^2 \\
&+84k*P_{1k}^{*}\varepsilon_1 h_1{}^{*5}\left(\frac{\mathrm{d}\Theta_{0I}^{1}(\eta)}{\mathrm{d}\eta}\right)^2 - 560k*P_{1k}^{*}\varepsilon_1 h_1{}^{*3}\left(\Theta_{0I}^{1}(\eta)\right)^2 \\
&+84k*P_{1k}^{*}\varepsilon_1 h_1{}^{*5}\Theta_{0I}^{1}(\eta)\frac{\mathrm{d}^2\Theta_{0I}^{1}(\eta)}{\mathrm{d}\eta^2}
\end{aligned}
\tag{35}
$$

The solution for Eqs. 33a-33b is similar to that of Eqs. 27a-27b. In the solution process of Eqs. 33a-33b since the answer in the regions far from the upper boundary (negative infinity) should have a limited value, the eigenvalues with a positive real part were chosen.

3.3 Composite Solution

Based on the matched expansion asymptotic perturbation technique, the composite solution $Y_{composite}$ is the sum of inner and outer solutions minus overlapping regions. Therefore, for the composite solution, we have:

$$Y_{composite} = Y_{outer} + Y_{inner} + Y_{Inner} - (Y_{outer})^{inner} - (Y_{outer})^{Inner} \tag{36}$$

$(Y_{outer})^{inner}$ and $(Y_{outer})^{Inner}$ are the common (same) parts of inner and outer solution in the boundary regions (near both heads of cylinder), which are obtained by Van Dyke matching principal [50]. By integrating the first component of composite solution, Θ^{0*} function is achieved ($\Theta^{0*}= (1/\varepsilon)\int \varsigma^* \, dx^* + K2$). By applying the boundary condition of Θ^{0*} in both heads of the cylinder, the $K1$ and $K2$ constants are determined.

4. Results and Discussion

For a numerical study, an FG cylinder with varying thickness is considered with geometric specifications are r_i =40 *mm*, h_a =20 *mm*, h_b =10 *mm*, h_0 =10 *mm*, and the length equal to 800*mm*. The inner layer of this FG cylinder is SUS304 and its properties in the positive reference temperature T_R=25°C is based on table 1 [47].

Table 1. Material property of inner layer of the FGM hollow cylinder

Properties of SUS304		Temperature dependency			
		P_{0i}	P_{1i} (1/°K)	P_{2i} (1/°K²)	P_{3i} (1/°K³)
k (W/(m °K))	15.379	1	-1.264×10⁻³	2.092×10⁻⁶	-7.223×10⁻¹⁰
α (10⁻⁶/°K)	12.33×10⁻⁶	1	8.086×10⁻⁴	0	0

The inner surface of FGM cylinder is heated by a heat flux equal 160 (W/m^2), and the outer surface of FGM cylinder is cooled by a heat flux equal 110 (W/m^2). In both heads of cylinder the constant temperature T=25°C is considered Moreover, in order to study the heterogeneity constant, n for values of 2, 1, 0, -1, and -2 is studied.

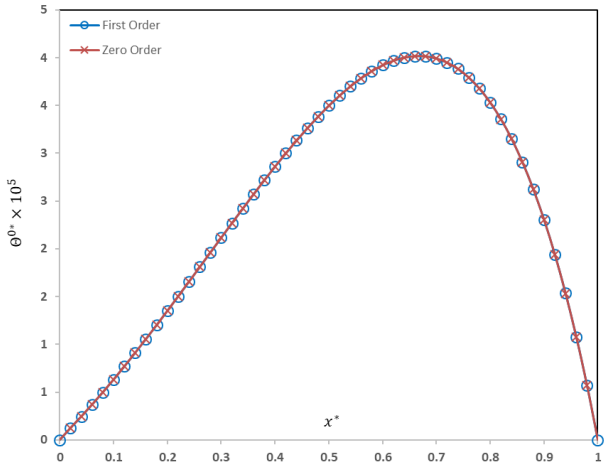

Figure 2. The zero-order components of temperature change for zero-order and first-order solution of perturbation term (n=1).

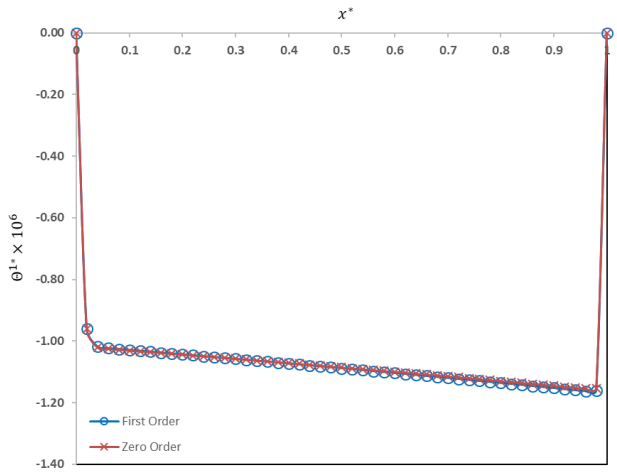

Figure 3. The first-order components of temperature change for zero-order and first-order solution of perturbation term (n=1).

Figures 2 and 3 shows Θ^{0*} and Θ^{1*} functions for zero-order and first-order solution of the perturbation term for Eq. 36. As it is seen the matched asymptotic expansion perturbation technique converges quickly and the first-order solution achieved from this method does not cause any significant modification to the functions.

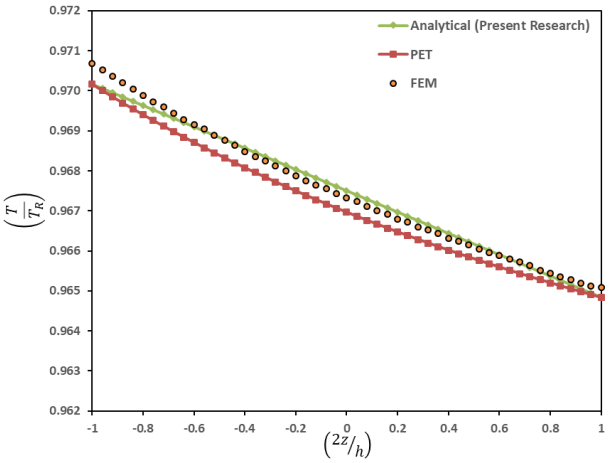

Figure 4. Distribution of temperature in the middle length of FGM cylinder with constant thickness (n=1).

In order to validate the results, the thickness of cylinder is constant at 20 *mm*. Moreover, it is assumed that material properties are temperature independent (P_{ji} = 0, j= 1, 2, 3). Fig.4 shows the distribution of temperature change in the FG cylinder. The results are predicted based on two analytical methods (present research and PET [28, 51-53]) and FEM.

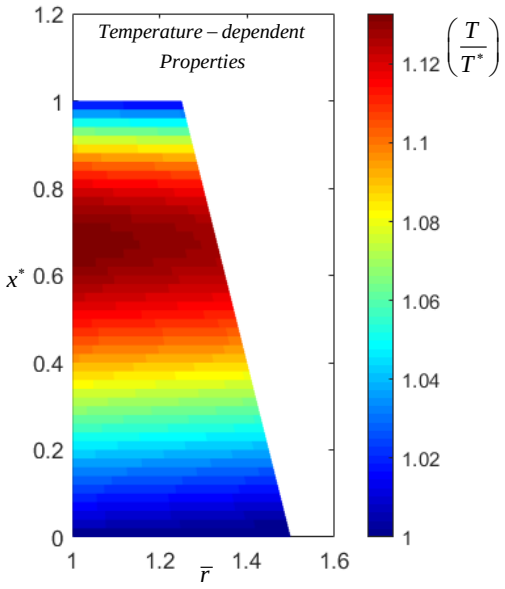

Figure 5. Dimensionless temperature distribution in FG cylinders (n=1) with variable thickness (temperature-dependency).

Figures 5 and 6 shows the temperature distribution in the FG cylinders with varying thickness for temperature-dependent and temperature-independent materials properties. Although the value of thermal loading in the inner and outer layers of FG cylinder is constant, considering the temperature-dependency of material slightly change the value of temperature distribution in the cylinder. The maximum temperature in the cylinder with properties temperature-dependent has been about 14 % more than the temperature of both heads of cylinder, resulting from temperature-dependency of material. It is worth noting, for considering the material properties is temperature-independent, it was assumed the P_{1k}, P_{2k}, and P_{3k} equal zero. In fact, in the low-temperature range, there is no need for nonlinear thermal analysis or consider the material properties are temperature-dependent since the effect of its slightly changes the result in structure.

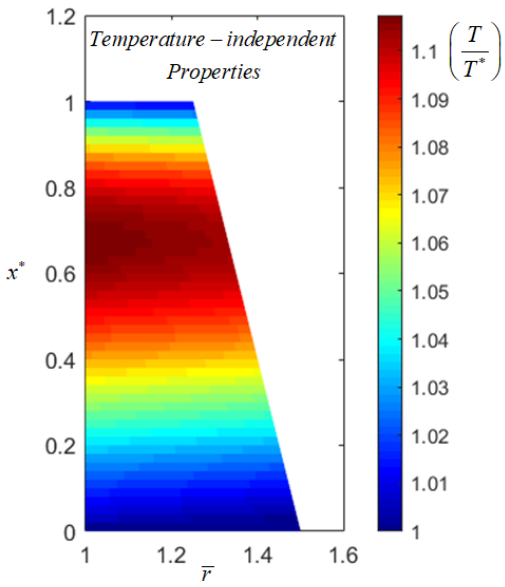

Figure 6. Dimensionless temperature distribution in FG cylinders with variable thickness (temperature-independency).

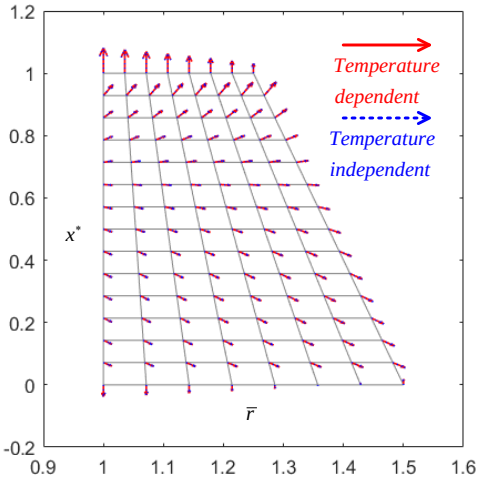

Figure 7. Dimensionless temperature distribution in FG cylinders (n=1) with variable thickness.

Figure 7 shows the heat flux distribution in FG cylinders for temperature-dependent materials properties (red arrow) and temperature-independent materials properties (blue arrow). As it is seen the direction of heat flux in the cylinders is independent from material temperature-dependency. In other words, linear thermal analyze or consider the material properties are temperature-independent can help to understand the path of heat flow in the FG cylinder that is a lot help, especially when the cylinder has contact with other components that affected by heat.

Figures 8 and 9 shows the thermal strain distribution in FG cylinders for temperature-dependent and temperature-independent materials properties. Although the value of thermal loading is constant, considering the temperature-dependency of material properties would slightly change the value of maximum thermal strain. Unlike the temperature field whose maximum value occurs in the inner layer, the maximum thermal strain occurred in the outer layer. Actually, the thermal expansion coefficient of the outer layer effect is much dominant than the maximum temperature in the inner layer.

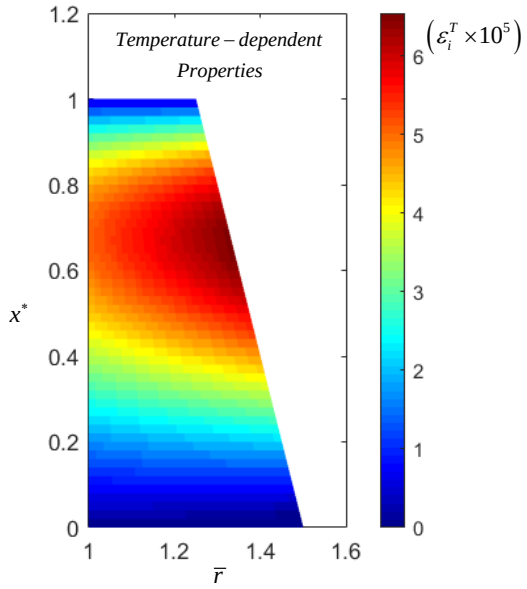

Figure 8. Thermal strain distribution in FG cylinders (n=1) with variable thickness (temperature-dependency).

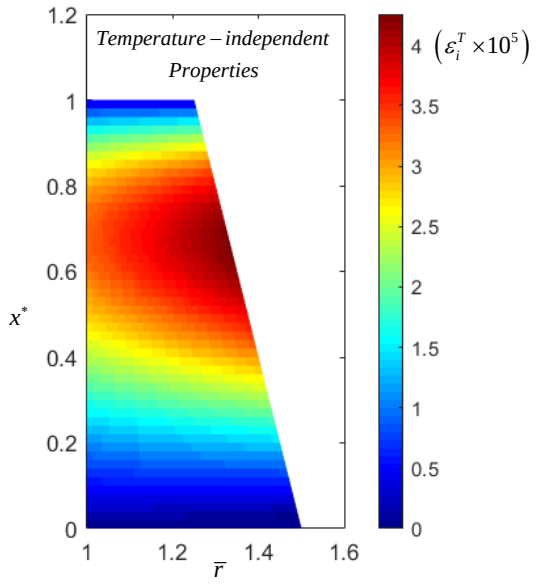

Figure 9. Thermal strain distribution in FG cylinders (n=1) with variable thickness (temperature-independency).

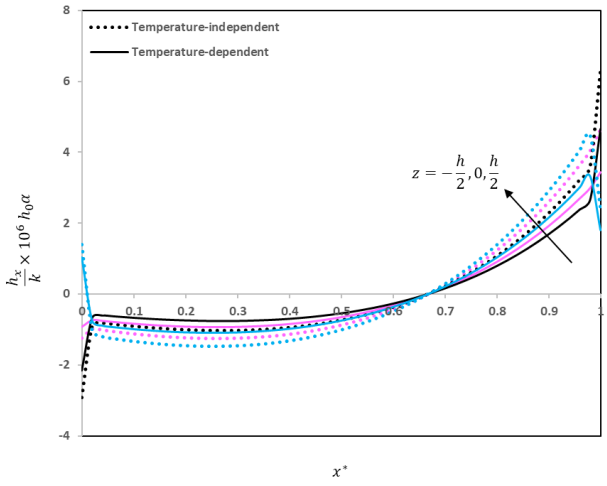

Figure 10. Axial component of heat flux in FG cylinder (n=1).

Figure 10 shows the axial component of heat flux in different layers of the FGM cylinder (n=1). Although, the direction of heat flux in the cylinders is same for linear and nonlinear thermal analyze the cylinder (figure 7) but the value of heat flux in nonlinear analysis is less than linear analysis.

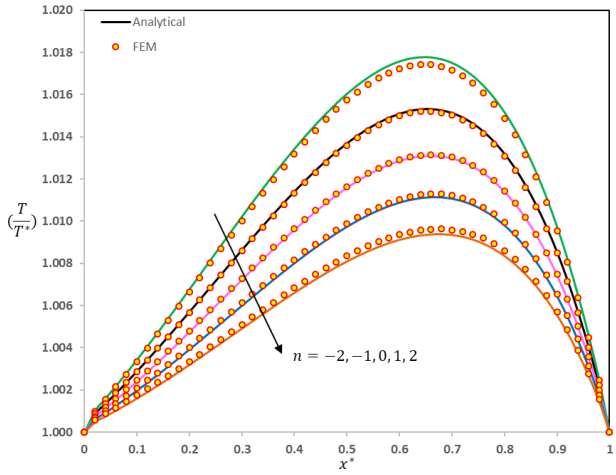

Figure 11. Temperature distribution in inner layer of FG cylinders.

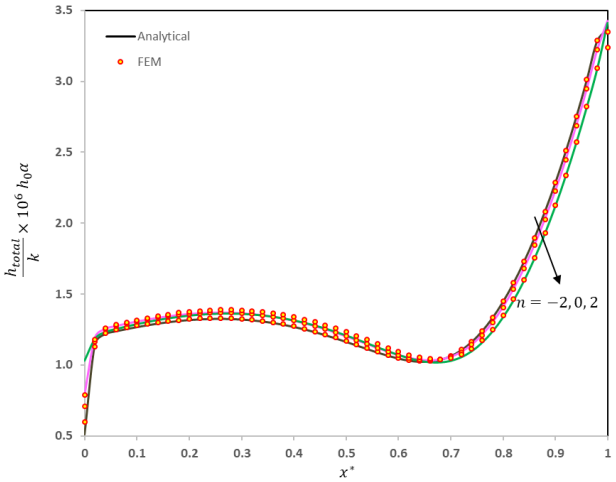

Figure 12. Distribution of heat flux in middle layer of FG cylinders.

Figure 11 shows the effect of heterogeneity on the temperature distribution in the inner layer of FG cylinders with varying thickness and temperature-dependent materials properties. As it is seen, any increase in the heterogeneity constant would lead to a decrease in the maximum value of temperature in the inner layer.

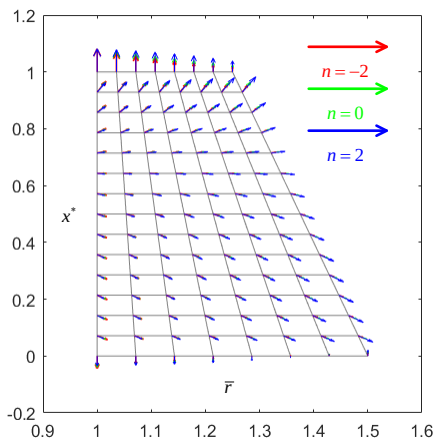

Figure 13. Distribution of heat flux inside the FG cylinders with variable thickness (temperature-dependency).

Figure 12 shows the total heat flux value distribution which has been calculated based on Eq. 37 in the middle layer of FG cylinders. Variations of heterogeneity constant do not lead to evident changes in the total heat flux value. Therefore the effect of heterogeneity constant on the total heat flux value can be ignored. The maximum value of total heat flux occurs in the boundary regions. It increases with any increase in the heterogeneity constant. Figure 13 shows the heat flux distribution in FG cylinders with varying thickness. As it is seen, variations of heterogeneity constant lead to a change only in the value (size) of heat flux vectors and have no effect on the heat flux vectors direction. Also, any increase in the heterogeneity constant could lead to an increase, decrease or no change in the heat flux value.

$$h_{total} = \sqrt{h_z^{\,2} + h_x^{\,2}} \tag{37}$$

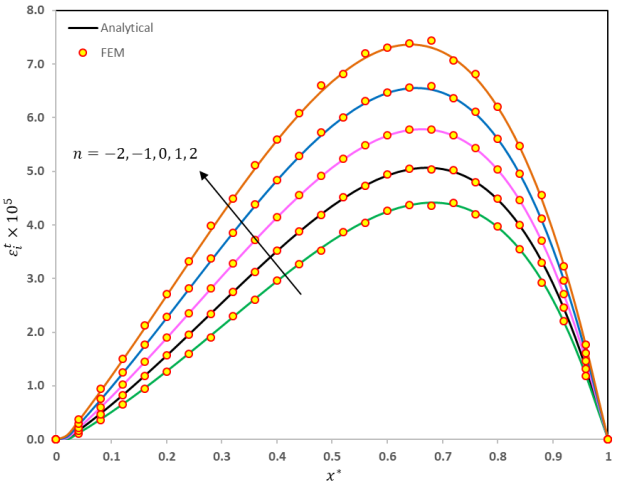

Figure 14. Distribution of thermal strain in outer layer of FG cylinders with variable thickness (temperature-dependency).

Figure 14 shows the thermal strain distribution in the outer layer of cylinders with varying thickness and temperature-dependent materials properties. The effect of heterogeneity constant on the thermal strain is demonstrative and any increase in the heterogeneity constant would increase the thermal strain value. Moreover, with any increase in the heterogeneity constant, the location of maximum thermal strain changes and approaches the lower head of cylinder.

5. Conclusion

In this study, the governing equations for FG cylinders with varying thickness and temperature-dependent materials properties which subjected to heat fluxes in the inner and outer layers were derived and a two-dimensional analytical solution was presented. A numerical study was performed for a cylinder with varying thickness with two heads with constant temperature and the effects of heterogeneity and the temperature-dependency properties were studied and evaluated. Furthermore, the results of this study were compared with previous study and FEM, and a good agreement was found between the results. The results of this study are summarized as follows.

1- The current research presents a two-dimensional analytic series solution for nonlinear heat conduction equation and thermal strain (considering the temperature-dependency of material properties), thereby requiring no special boundary conditions in both cylinder heads with respect to other series solutions, and they converge fast. It is clear that this solution can be used as an objective function to optimize and achieve optimal values such as thickness change profile and heterogeneity constant.

2. The investigation and evaluation of the results of nonlinear thermal analysis of cylinders with varying thickness shows that considering the temperature-dependency of material, in the low-temperature range slightly change the value of temperature and thermal strain distribution in the cylinder but heat flux directions in the body don't change. Therefore, if the purpose is to understand the behavior of heat flow in the cylinder, linear thermal analysis is adequate but to realize the temperature and thermal strain distribution, considering the temperature-dependency of material properties is necessary and nonlinear analysis should be done.

3. The study of results shows that in the FG cylinders with varying thickness, necessarily the maximum thermal strain is not necessarily located in the maximum temperature location. It may be in other locations, depending on how properties like thermal expansion coefficient are distributed in cylinder.

4. The results show that the heterogeneity constant has demonstrative effects on the temperature field and the thermal strain created inside the cylinder with varying thickness. As the heterogeneity constant increases, the temperature field decreases in the cylinder, but the thermal strain increases in the cylinder.

5. The results show that variations of heterogeneity constants do not significantly change the amount of heat flux inside the FG cylinders and do not change the direction of the heat flux vector either.

References

[1] Zhao X., Zhang Z.M., Zhang B.H., 2014, Research on rolling–extrusion forming of variable wall thickness cylinder parts, Materials Research Innovations 18(2): S2-940-S2-945.

[2] Grigorenko A.Y., Müller W.H., Grigorenko Y.M., Vlaikov G.G., 2016, Recent Developments in Anisotropic Heterogeneous Shell Theory: Applications of Refined and Three-dimensional Theory—Volume IIB, Springer.

[3] Kasaeian A., Vatan S.N., Daneshmand S., 2011, FGM materials and finding an appropriate model for the thermal conductivity, Procedia engineering (14): 3199-3204.

[4] Li W., Han B., Research and Application of Functionally Gradient Materials, in: IOP Conference Series: Materials Science and Engineering, IOP Publishing, 022065.

[5] Dai H-L., Rao Y-N., Dai T., 2016, A review of recent researches on FGM cylindrical structures under coupled physical interactions, 2000–2015, Composite Structures 152: 199-225.

[6] Zimmerman R.W., Lutz M.P., 1999, Thermal stresses and thermal expansion in a uniformly heated functionally graded cylinder, Journal of Thermal Stresses 22(2): 177-188.

[7] Awaji H., Sivakumar R., 2001, Temperature and Stress Distributions in a Hollow Cylinder of Functionally Graded Material: The Case of Temperature-Independent Material Properties, Journal of the American Ceramic Society 84(5): 1059-1065.

[8] El-Naggar A., Abd-Alla A., Fahmy M., Ahmed S., 2002, Thermal stresses in a rotating non-homogeneous orthotropic hollow cylinder, Heat and Mass Transfer 39(1): 41-46.

[9] Shao Z., 2005, Mechanical and thermal stresses of a functionally graded circular hollow cylinder with finite length, International Journal of Pressure Vessels and Piping 82(3): 155-163.

[10] Ruhi M., Angoshtari A., Naghdabadi R., 2005, Thermoelastic analysis of thick-walled finite-length cylinders of functionally graded materials, Journal of Thermal Stresses 28(4): 391-408.

[11] Ootao Y., Tanigawa Y., 2006, Transient thermoelastic analysis for a functionally graded hollow cylinder, Journal of Thermal Stresses 29(11): 1031-1046.

[12] Shao Z., Ma G., 2008, Thermo-mechanical stresses in functionally graded circular hollow cylinder with linearly increasing boundary temperature, Composite Structures 83(3): 259-265.

[13] Bahtui A., Eslami M., 2007, Coupled thermoelasticity of functionally graded cylindrical shells, Mechanics research communications 34(1): 1-18.

[14] Akbari Alashti R., Khorsand M., Tarahhomi M., 2012, Asymmetric thermo-elastic analysis of long cylindrical shells of functionally graded materials by differential quadrature method, Proceedings of the Institution of Mechanical Engineers, Part C: Journal of Mechanical Engineering Science 226(5): 1133-1147.

[15] Tokovyy Y.V., Ma C.-C., 2008, Analysis of 2D non-axisymmetric elasticity and thermoelasticity problems for radially inhomogeneous hollow cylinders, Journal of Engineering Mathematics 61(2-4): 171-184.

[16] Peng X., Li X., 2010, Thermoelastic analysis of a cylindrical vessel of functionally graded materials, International journal of pressure vessels and piping 87(5): 203-210.

[17] Chang W.-J., Lee H.-L., Yang Y.-C., 2011, Estimation of heat flux and thermal stresses in functionally graded hollow circular cylinders, Journal of Thermal Stresses 34(7): 740-755.

[18] Aziz A., Torabi M., 2013, Thermal stresses in a hollow cylinder with convective boundary conditions on the inside and outside surfaces, Journal of Thermal Stresses 36(10): 1096-1111.

[19] Xin L., Dui G., Yang S., Zhou D., 2015, Solutions for behavior of a functionally graded thick-walled tube subjected to mechanical and thermal loads, International Journal of Mechanical Sciences 98: 70-79.

[20] M. Ghannad, M. Parhizkar Yaghoobi, 2015, A thermoelasticity solution for thick cylinders subjected to thermo-mechanical loads under various boundary conditions, International Journal of Advanced Design and Manufacturing Technology 8(4): 1-12.

[21] M. Ghannad, M. Parhizkar Yaghoobi, 2017, 2D thermo elastic behavior of a FG cylinder under thermomechanical loads using a first order temperature theory, International Journal of Pressure Vessels and Piping 149: 75-92.

[22] Daneshmehr A., Rajabpoor A., Hadi A., 2015, Size dependent free vibration analysis of nanoplates made of functionally graded materials based on nonlocal elasticity theory with high order theories, International Journal of Engineering Science 95: 23-35.

[23] Zamani Nejad M., Hadi A., 2016, Non-local analysis of free vibration of bi-directional functionally graded Euler–Bernoulli nano-beams, International Journal of Engineering Science 105: 1-11.

[24] Zamani Nejad M., Hadi A., 2016, Eringen's non-local elasticity theory for bending analysis of bi-directional functionally graded Euler–Bernoulli nano-beams, International Journal of Engineering Science 106: 1-9.

[25] Zamani Nejad M., Hadi A., Rastgoo A., 2016, Buckling analysis of arbitrary two-directional functionally graded Euler–Bernoulli nano-beams based on nonlocal elasticity theory, International Journal of Engineering Science 103: 1-10.

[26] Zamani Nejad M., Jabbari M., Hadi A., 2017, A review of functionally graded thick cylindrical and conical shells, Journal of Computational Applied Mechanics 48(2): 357-370.

[27] Khoshgoftar M., Ghorbanpour Arani A., Arefi M., 2009, Thermoelastic analysis of a thick walled cylinder made of functionally graded piezoelectric material, Smart Materials and Structures 18(11): 115007.

[28] Ghorbanpour A., Loghman A., Abdollahitaheri A., Atabakhshian V., 2011, Electrothermomechanical behavior of a radially polarized rotating functionally graded piezoelectric cylinder, Journal of Mechanics of Materials and Structures 6(6): 869-882.

[29] Parhizkar Yaghoobi M., Ghaffari I., Ghannad M., 2018, Stress and active control analysis of functionally graded piezoelectric material cylinder and disk under electro-thermo-mechanical loading, Journal of Intelligent Material Systems and Structures 29(5) 924-937.

[30] Atrian A., Fesharaki J.J., Nourbakhsh S., 2015, Thermo-electromechanical behavior of functionally graded piezoelectric hollow cylinder under non-axisymmetric loads, Applied Mathematics and Mechanics 36(7): 939-954.

[31] Loghman A., Nasr M., Arefi M., 2017, Nonsymmetric thermomechanical analysis of a functionally graded cylinder subjected to mechanical, thermal, and magnetic loads, Journal of Thermal Stresses 40(6): 765-782.

[32] Meshkini M., Firoozbakhsh K., Jabbari M., SelkGhafari A., 2017, Asymmetric mechanical and thermal stresses in 2D-FGPPMs hollow cylinder, Journal of Thermal Stresses, 40(4): 448-469.

[33] Zamani Nejad M., Hadi A., Farajpour A., 2017, Consistent couple-stress theory for free vibration analysis of Euler-Bernoulli nano-beams made of arbitrary bi-directional functionally graded materials, Structural Engineering and Mechanics 63(2): 161-169.

[34] Hadi A., Zamani Nejad M., Hosseini M., 2018, Vibrations of three-dimensionally graded nanobeams, International Journal of Engineering Science 128: 12-23.

[35] Hadi A., Zamani Nejad M., Rastgoo A., Hosseini M., 2018, Buckling analysis of FGM Euler-Bernoulli nano-beams with 3D-varying properties based on consistent couple-stress theory, Steel and Composite Structures 26(6): 663-672.

[36] Zamani Nejad M., Hadi A., Omidvari A., Rastgoo A., 2018, Bending analysis of bi-directional functionally graded Euler-Bernoulli nano-beams using integral form of Eringen's non-local elasticity theory, Structural Engineering and Mechanics 67(4): 417-425.

[37] Ghaffari I., Parhizkar Yaghoobi M., Ghannad M., 2018, Complete mechanical behavior analysis of FG Nano Beam under non-uniform loading using non-local theory, Materials Research Express 5(1): 015016.

[38] Zarezadeh E., Hosseini V., Hadi A., 2019, Torsional vibration of functionally graded nano-rod under magnetic field supported by a generalized torsional foundation based on nonlocal elasticity theory,

Mechanics Based Design of Structures and Machines: 1-16.

[39] Barati A., Adeli M.M., Hadi A., 2020, Static torsion of bi-directional functionally graded microtube based on the couple stress theory under magnetic field, International Journal of Applied Mechanics 12(02): 2050021.

[40] Dehshahri K., Zamani Nejad M., Ziaee S., Niknejad A., Hadi A., 2020, Free vibrations analysis of arbitrary three-dimensionally FGM nanoplates, Advances in nano research 8(2): 115-134.

[41] Barati A., Hadi A., Zamani Nejad M., Noroozi R., 2020, On vibration of bi-directional functionally graded nanobeams under magnetic field, Mechanics Based Design of Structures and Machines: 1-18.

[42] Noroozi R., Barati A., Kazemi A., Norouzi S., Hadi A., 2020, Torsional vibration analysis of bi-directional FG nano-cone with arbitrary cross-section based on nonlocal strain gradient elasticity, Advances in nano research 8(1): 13-24.

[43] Ghannad M., Rahimi G.H., Zamani Nejad M., 2013, Elastic analysis of pressurized thick cylindrical shells with variable thickness made of functionally graded materials, Composites Part B: Engineering 45(1): 388-396.

[44] Jabbari M., Zamani Nejad M., 2018, Mechanical and thermal stresses in radially functionally graded hollow cylinders with variable thickness due to symmetric loads, Australian Journal of Mechanical Engineering: 1-14.

[45] Zamani Nejad M., Jabbari M., Ghannad M., 2017, A general disk form formulation for thermo-elastic analysis of functionally graded thick shells of revolution with arbitrary curvature and variable thickness, Acta Mechanica 228(1): 215-231.

[46] Mehditabar A., Rahimi G.H., Fard K.M., 2018, Thermoelastic Analysis of Rotating Functionally Graded Truncated Conical Shell by the Methods of Polynomial Based Differential Quadrature and Fourier Expansion-Based Differential Quadrature, Mathematical Problems in Engineering 2018.

[47] Wang Y., Liu D., Wang Q., Zhou J., 2018, Thermoelastic interaction in functionally graded thick hollow cylinder with temperature-dependent properties, Journal of Thermal Stresses 41(4): 399-417.

[48] Benjeddou A., Andrianarison O., 2005, A thermopiezoelectric mixed variational theorem for smart multilayered composites, Computers & Structures 83(15-16): 1266-1276.

[49] Mahboubi Nasrekani F., Eipakchi H., 2015, Nonlinear Analysis of Cylindrical Shells with Varying Thickness and Moderately Large Deformation under Nonuniform Compressive Pressure Using the First-Order Shear Deformation Theory, Journal of Engineering Mechanics 141(5): 04014153.

[50] Nayfeh A.H., 2011, Introduction to perturbation techniques, John Wiley & Sons.

[51] Omidi Bidgoli M., Arefi M., Loghman A., 2018, Thermoelastic behaviour of FGM rotating cylinder resting on friction bed subjected to a thermal gradient and an external torque, Australian Journal of Mechanical Engineering: 1-9.

[52] Omidi Bidgoli M., Loghman A., Arefi M., 2019, The Effect of Grading Index on Two-dimensional Stress and Strain Distribution of FG Rotating Cylinder Resting on a Friction Bed Under Thermomechanical Loading, Journal of Stress Analysis 3(2): 75-82.

[53] Omidi Bidgoli M., Loghman A., Arefi M., 2019, Three-Dimensional Thermo-Elastic Analysis of a Rotating Cylindrical Functionally Graded Shell Subjected to Mechanical and Thermal Loads Based on the FSDT Formulation, Journal of Applied Mechanics and Technical Physics 60(5) 899-907.